energies

MDPI

Article

Implementation of a Novel Tabu Search Optimization Algorithm to Extract Parasitic Parameters of Solar Panel

Naveena Bhargavi Repalle [1,*], Pullacheri Sarala [2], Lucian Mihet-Popa [3,*], Shashidhar Reddy Kotha [1] and Nagalingam Rajeswaran [4]

[1] Electrical and Electronics Engineering, CVR College of Engineering, Hyderabad 501510, India; shashidhar.kotha5@gmail.com
[2] Electrical and Electronics Engineering, Malla Reddy Engineering College, Maisammaguda, Secunderabad 500100, India; sarala.2906@gmail.com
[3] Faculty of Information Technology, Engineering and Economics, Oestfold University College, 1757 Halden, Norway
[4] Electrical and Electronics Engineering, Malla Reddy Institute of Engineering and Technology, Maisammaguda, Secunderabad 500100, India; rajeswarann@gmail.com
* Correspondence: bhargavi.rn5@gmail.com (N.B.R.); lucian.mihet@hiof.no (L.M.-P.)

Abstract: The aging of PV cells reduces their electrical performance i.e., the parasitic parameters are introduced in the solar panel. The shunt resistance (R_{Sh}), series resistance (R_S), photo current (I_{Ph}), diode current (I_d), and diffusion constant (a_1) are known as parasitic or extraction parameters. Cracks and hotspots reduce the performance of PV cells and result in poor V–I characteristics. Certain tests are carried out over a long period of time to determine the quality of solar cells; for example, 1000 h of testing is comparable to 20 years of operation. The extraction of solar parameters is important for PV modules. The Tabu Search Optimization (TSO) algorithm is a robust meta-heuristic algorithm that was employed in this study for the extraction of parasitic parameters. Particle Swarm Optimization (PSO) and a Genetic lgorithm (GA), as well as other well-known optimization methods, were used to test the proposed method's correctness. The other approaches included the lightning search algorithm (LSA), gravitational search algorithm (GSA), and pattern search (PS). It can be concluded that the TSO approach extracts all six parameters in a reasonably short period of time. The work presented in this paper was developed and analyzed using a MATLAB-Simulink software environment.

Keywords: synthetic data (SD); pattern search (PS); absolute error; optimization technique; solar cell (SC); tabu list (TL)

Citation: Repalle, N.B.; Sarala, P.; Mihet-Popa, L.; Kotha, S.R.; Rajeswaran, N. Implementation of a Novel Tabu Search Optimization Algorithm to Extract Parasitic Parameters of Solar Panel. *Energies* **2022**, *15*, 4515. https://doi.org/10.3390/en15134515

Academic Editors: Bruno Canizes, João Soares, Sérgio Ramos and Zahra Foroozandeh

Received: 23 May 2022
Accepted: 19 June 2022
Published: 21 June 2022

1. Introduction

Photovoltaic (PV) systems are ecologically benign, cost-effective, and simple to incorporate into traditional electricity grids [1]. To diminish power lopsidedness, sunlight-based chargers are not straightforwardly connected to the load [2]. A panel-to-load power tracking strategy is recommended to avoid this problem [3]. Another major area of study is the extraction of parasitic features from the solar cell [4]. In this article, the use of the TSO approach to extract solar properties is reported.

PV systems with one diode were studied mathematically by Villalva et al. [5]. The suggested modelling is easily accessible, quick, meticulous, and emulation-friendly. Series and shunt protections, as well as how the continuous functional cluster thinks about as far as most extreme power [6], are considered in the plan. Three aspects are focused to modify the nonlinear condition contingent upon the I–V bend in an experimental manner [7].

On a solitary-diode model of a sunlight-based cell, X. Mama et al. [8] recommended an information-driven I–V strategy that was surveyed on three boundaries (short circuit current (ISC), RSh, and open-circuited voltage, VOC). For finding plan boundaries, such as ideally consistent RS, RP, photon initiation current, and dull current, Saleem et al. [9] proposed a four-point extraction procedure [9]. Using GaAsP and SiGe tandem structures with a three-terminal assessment [10], the authors were able to derive sub-cell features. An analysis of the potential difference between the two reference cells was used to derive individual voltages in the proposed method.

Predicting the losses of sub-passive cells also alters I–V curves. Consequently, different, but similar, conditions at various input bands [11] govern the multi-performance junction's performance. Particle swarm optimization (PSO) was laid out by Wei et al. [12] to segregate the exhibition attributes of natural sun-oriented cells, combined with three-diode lumped boundaries. Muralidhar et al. [13] proposed a technique that assists with overcoming the deficiency to avoid the drifting of local optimum issues. Diab et al. [14] researched and proposed a quick and precise method for separating obscure sun-oriented properties involving tree growth algorithm for assorted sun-powered PV modules. This strategy guarantees that all recovered boundaries are processed under ideal circumstances, bringing about optimal outcomes. In the future extension for this , PV systems will be able to make use of this method in partially shaded conditions [15].

In Raba et al. [16], a definite Markov chain Monte Carlo approach was used to prove that 2-dimensional organic solar cells were devoid of uncontrolled events. Caracciolo et al. [17] developed a single-variable optimization technique for constant environmental conditions. It was found that the majority of the features, such as the R_{Sh}, IO, and panel range, were resolved when tested under extreme environmental conditions. Therefore, the proposed method is successful in all challenging circumstances.

Cervellini et al. [18] and Semero et al. [19] suggested a novel genetic algorithm (GA) that can be applied to a wide range of kelvins and irradiation (G) zones [20]. The simple and easy expression of the I–V curve and accompanying equations is achieved using the recommended GA approach [20]. This simplifies the assessment process. For single-, double-, and multi-diode plans, Liao et al. [21] developed difference vector in differential evolution with adaptive mutation. DVADE's goal is to quickly determine the extricated limits of a broad range of PV models. Each individual vector is used and reused in the mutation technique, which employs a differential evolution process and, therefore, may be reused many times. Toledo et al. proposed the two-step linear-least-square technique [22]. There is a vital benefit to the recommended approach, which is that it can gather information whether it is obtained from an I–V curve, i.e., it does not need any previous assessments and does not request information on past examinations or data about the boundaries [23,24]. It is feasible to eliminate the inherent potential (Vbi) from cells by utilizing a material-science-based model and an observational method considering I–V attributes [25,26].

The following is a summary of the remaining portion of the paper. Following the introduction, Section 2 presents a mathematical depiction of a solar panel. Section 3 illustrates the ageing effect of the solar panel. In Section 4, proposed methods are presented. Section 5 provides a comparison of the suggested method's findings and performance with those of existing meta-heuristics. Conclusions and recommendations are provided in Section 6.

2. Mathematical Modeling of PV Cell Based on Single Diode

The current produced by the sunlight is parallelized utilizing the current source from a single-diode-modeled solar cell (SC), with the diode acting as a half-wave rectifier. The model is easy to implement due to its simplest form. However, this model does not give the required information regarding the solar cell's parameters [27]. Figure 1 shows the equivalent circuit of a single-diode-modeled SC.

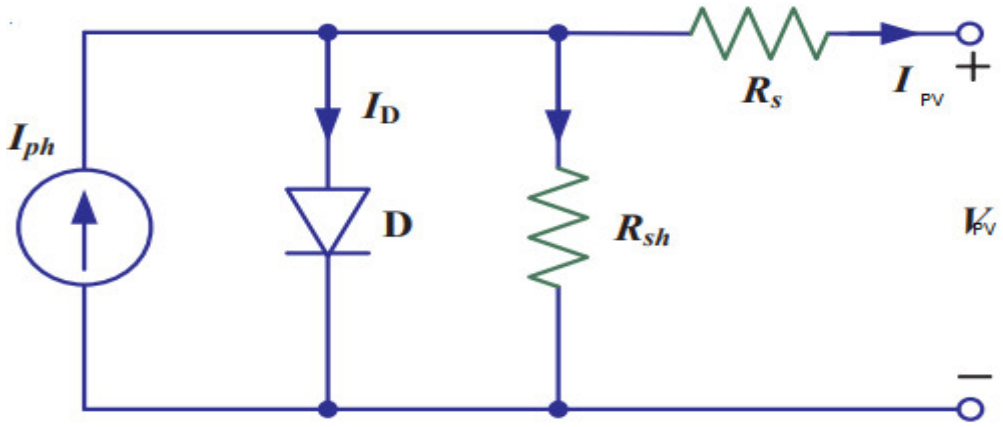

Figure 1. Circuit diagram of a single-diode-modeled solar cell.

The PV current obtained from the sunlight-based charger was determined as follows:

$$I_{PV} = I_{Ph} - I_d \tag{1}$$

where I_{PV} is the photovoltaic current, I_{Ph} is the photo current, and I_d is the diode current. The I_d was obtained based on Shockley equation, which is represented as:

$$I_d = I_S\left[\exp\left(\frac{q(V_{PV} + I_{PV}R_S}{\eta K_b T_k}\right) - 1\right] \tag{2}$$

The output current of the PV cell is represented as follows:

$$I_{PV} = I_{Ph} - I_S\left[\exp\left(\frac{q(V_{PV} + I_{PV}R_S)}{\eta K_b T_k}\right) - 1\right] - \tag{3}$$

The following implicit form simplifies the PV cell's output characteristics:

$$F(I_{PV}, V_{PV}, T_K, G) = I_{Ph} - I_{PV} - I_S[\alpha_1] - \beta_1 \tag{4}$$

$$\left.\begin{array}{l} where \quad \alpha_1 = \exp\left(\frac{q(V_{PV} + I_{PV}R_S)}{\eta K_b T_k}\right) - 1 \\ \beta_1 = \frac{V_{PV} + I_{PV}R_S}{R_P} \end{array}\right\} \tag{5}$$

3. Aging Effect of Solar Panels

The aging of the PV module depends on the type of photovoltaic technology employed for the design of the solar cell and the environmental conditions in which it is installed. The PV panel performance is degraded due to the formation of cracks and bubbles on the panel surface. The performance of solar panels is reduced due to aging, which is mainly due to dust accumulation, humidity, UV radiation, wind speed, temperature, and certain other external factors, such as rain, snow, hail, and mechanical shocks.

Impact of Aging on Solar Cell

The aging of the PV cell reduces the electrical performance, i.e., the parasitic parameters are introduced in the solar panel. The shunt resistance (R_{Sh}), series resistance (R_S), photo current (I_{Ph}), diode current (I_d), and diffusion constant (a_1) are known as parasitic or

extraction parameters. Cracks and hotspots reduce the performance of solar panel V–I characteristics. Certain tests are carried out over a span of time to determine the quality of solar cells; for example, 1000 h of testing is comparable to 20 years of operation [28].

The aging of the PV panel is described using aging laws, which are represented as follows:

$$\tau_1(T) = \tau_0(-\alpha_{opt}.T + 100\%) \quad (6)$$

$$R_S(T) = R_{S0} + (\alpha_{RS}.T + 100\%) \quad (7)$$

where α_{opt} represents the degradation rates of the transmissivity (glass optical losses and encapsulating losses) and the α_{R_S} of the series resistance (the deterioration of the electrical parts) are defined with accelerated test results. The degradation laws, the reduction in the transmissivity, and the augmentation of the series resistance according to time are given by expressions (6) and (7). The obtained degradation coefficients are α_{opt} = 0.6% per year and α_{R_S} = 0.23% per year. τ is the transmissivity and *T* is the time in years.

4. Proposed Tabu Search Optimization (TSO) Algorithm

To address the state of the issue of numerous optimizations, the meta-heuristic method is applied. During optimization, the lowest value is chosen initially, followed by a more extensive search. The tabu list (TL) memory utilitarian strategy obtains the information and stores the past arrangement while directing the following stage. For forestalling nearby improvements, irrelevant information is limited, and ideal information is isolated in aspiration criteria (AC). It is feasible to involve nearby heuristic examination tasks to concentrate on the outcome space in front of the neighborhood ideal through the TSO approach, which utilizes TL to help achieve developmental memory with appropriate limitations and goal levels.

To solve finite-solution set optimization problems, dynamic properties research is preferred because of the flexible memory consumption in tabu motions. Repeated solutions are out of the question, since these are unrepeatable activities. There are three varieties of TSO: the forbidding strategy, the freeing strategy system, and the short-term strategy (STS). By performing approximated solutions, the STS maintains a link between the FS and the FSS, while the FSS takes care of what remains after the optimization process, and the FS controls which data reach the operational zone. Figure 2 portrays the forbidden development, which depends on non-improved and nonlinear arrangements, as well as memory and neighborhood arrangements.

The TL should not contain any of these options. The tabu classification may be discarded if new tabu motions are introduced.

The new set of T(S) solutions is as follows:

$$S^l \in N(S) = \{(N(S) - T(S)\} + A(S) \quad (8)$$

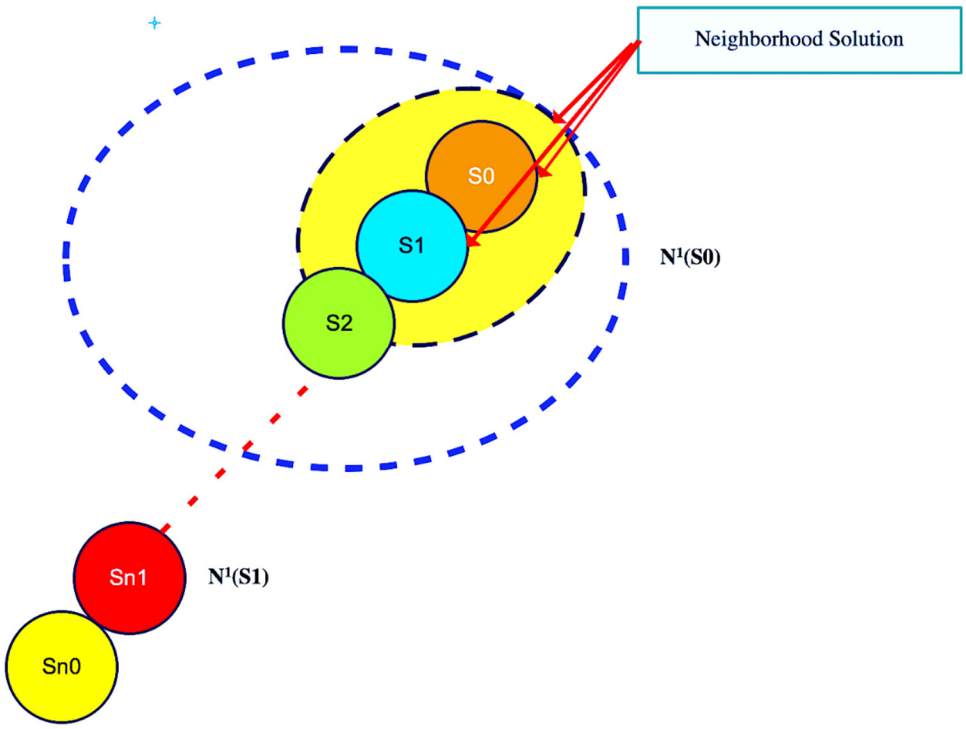

Figure 2. Tabu list neighborhood solutions for new solution.

TSO integrates goal programming and evaluates the solutions in more than one dimension, i.e., comparing the most important value with the first, second, third, and so on. The TSO framework is depicted in Figure 3.

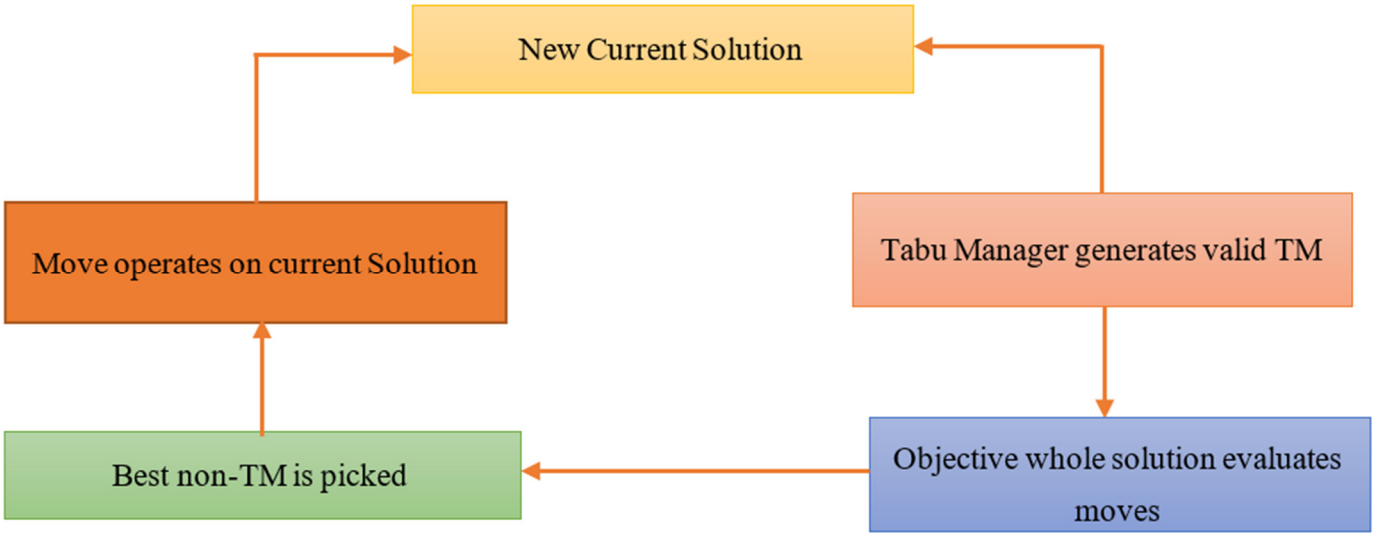

Figure 3. TSO framework for obtaining the optimal solution.

Basic TSO

The algorithm (Algorithm 1) for Basic Tabu Search Optimation is detailed step wise below.

Algorithm 1 Basic TSO	
STEP 1	Select a primary result i_o in S. Set i_0*= 0 and k = 0.
STEP 2	Fix k = k + 1 and produce a subset V* of outcomes in N (i_0, k) in such a way that either one of the tabu circumstances is infringed, or even one of the aspiration conditions is clutched.
STEP 3	Select the best j in V* and put i_0= j.
STEP 4	If f (i_0) < f (i_0*) arrange i_0*= i_0.
STEP 5	Update tabu and aspirational conditions.
STEP 6	Stop if a stopping condition is reached. Otherwise, go to STEP 2.
STEP 7	The stopping criteria of TS are as follows: N (i, k + 1) = 0. i.e., no possible resolution in the vicinity of result i_0. Here, k is largest than the highest numbers of rearrangements that are accepted. The number of repetitions since the last advancement of i_0* is higher than the corresponding number. There is confirmation that an optimal result has been obtained.

The upper-band and lower-band areas are described by feasible and unfeasible parameters. The number of generations is determined by the feasibility, as indicated in Figure 4a,b.

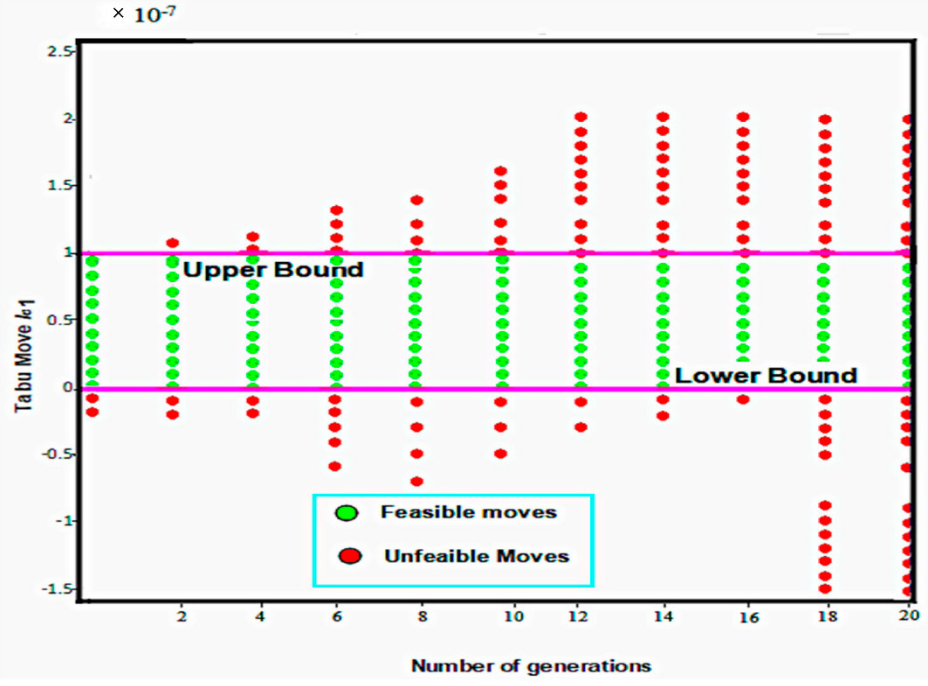

(**a**)

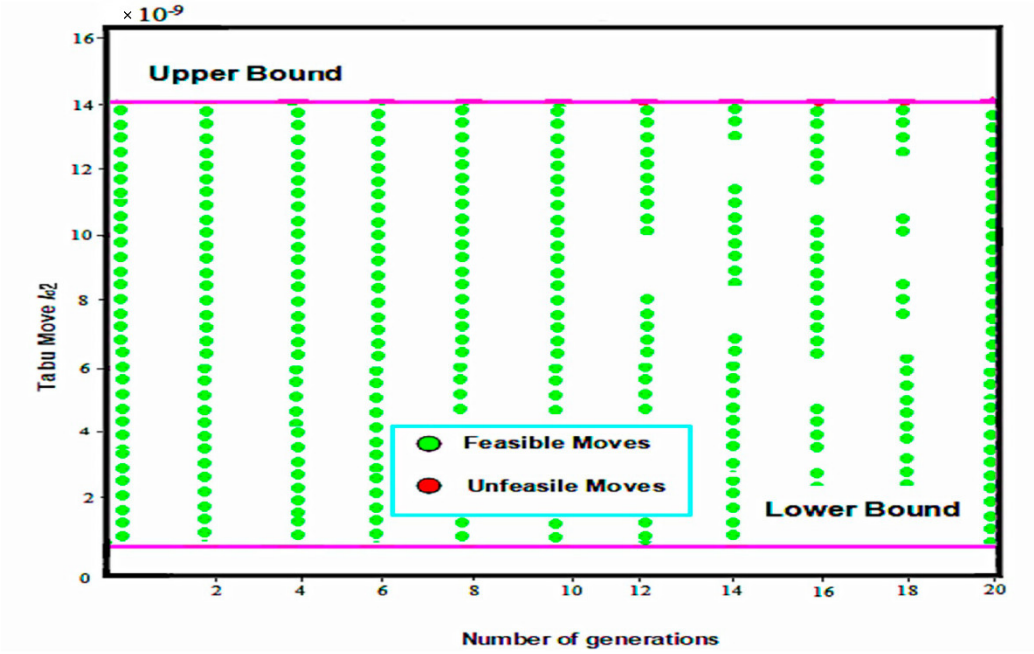

(**b**)

Figure 4. Resulting tabu movements. (**a**) Lower feasibility and (**b**) higher feasibility.

5. Results and Analysis

The numerical re-enactments of the proposed strategy were simulated in MATLAB/Simulink along with existing methods such as LSA and GSA. The obtained numerical findings and synthetic data (SD) had a significant connection. A comparison of the proposed TSO algorithm's performance on two different solar-panel wattage ranges was drawn. On Windows XP, with a 1.2 GHz Mobile Intel CPU, all of the algorithms ran on a single platform with distinct basic data. The proficiency of the boundary extraction strategy was assessed utilizing the assembly, I–V information bend, and calculation execution.

In this work, to extract the parameters, real measured V–I data of the solar cell and PV module were used in the simulation. A commercial silicon solar cell 57 mm in diameter was taken as the prototype and V–I measurements were taken under one sun (100 W/m^2) at 33 °C. This prototype is the same as that used by AlRashidi et al. (2011) and AlHajri et al. (2012). The adjustable parameters in this simulation, determined by trial, were given by: population size (parallel number) N = 100, maximum iteration number kmax = 2500, crossover operation rate Pc = 0:5, and merging operation rate Pm = 0:5.

The information examination of a 40-watt PV board is displayed in Table 1. The values derived using the GA algorithm for the parameters I_{Ph}, I_{01}, I_{02}, R_S, R_P, and a1 were 2.69 A, 9.51 * 10^{-9} A, 32 × 10^{-7} A, 0.0794 Ω, 878.95 Ω, and 1.28. In addition, the suggested TSO method extracted 1.94 A (I_{Ph}), 6.35 × 10^{-9} A (I01), 11.92 × 10^{-7} A (I02), 0.0782 Ω (R_S), 762.68 Ω (R_P), and 1.29 A (I_{Ph}) (a1). The analysis of the pre-existing synthetic data with the numerical values gathered by the various instruments used in this study clearly yielded a statistically significant difference. When compared to other current algorithms, the TSO algorithm requires substantially less time to compute, taking just 112 s.

Table 2 shows that the suggested TSO method produced numerical results that were similar to the synthetic data, namely 5.41 A (I_{Ph}), 8.7 × 10^{-9} A (I01), 9.29 × 10^{-5} A (I_{02}), 0.942 Ω (R_S), 1281.98 Ω (R_P), and 1.01 A (I_{Ph}) (a1). When compared to current techniques, the TSO algorithm takes less time to compute (228 s). Accordingly, the proposed TSO calculation was demonstrated to be better than that of current metaheuristic calculations. Figure 5a–d shows the I–V charts of the S75, S115, SM55, and SQ150PC modules utilizing the TSO technique and test information, respectively.

Table 1. Comparison of fata for a 40-watt PV panel using GA, LSA, GSA, PS, PSO, and proposed TSO algorithms.

S.NO	Parameter	Synthetic Data	GA	LSA	GSA	PS	PSO	TSO
1	I_{ph}	1.967 A	2.69 A	2.55 A	2.162 A	2.189 A	2.01 A	1.94 A
2	I_{01}	6.23×10^{-9} A	9.51×10^{-9} A	8.2×10^{-9} A	8.6×10^{-9} A	7.65×10^{-9} A	5.65×10^{-9} A	6.35×10^{-9} A
3	I_{02}	20.9×10^{-7} A	32.6×10^{-7} A	25.9×10^{-7} A	26.28×10^{-7} A	26.76×10^{-7} A	23.32×10^{-7} A	11.92×10^{-7} A
4	R_s	0.0775 Ω	0.0794 Ω	0.0975 Ω	0.097 Ω	0.0969 Ω	0.0954 Ω	0.0782Ω
5	R_p	712.65 Ω	878.95 Ω	862.65 Ω	858.53 Ω	816.76 Ω	782.65 Ω	762.68 Ω
6	a_1	1.45	1.28	1.19	1.32	1.47	1.38	1.29
7	Time (s)	…	779	682	395	362	237	112

Table 2. Comparison of data for a 200-watt PV panel using Ga, Lsa, Gsa, Ps, Pso, and proposed TSO algorithms.

S.No.	Parameter	Synthetic data	GA	LSA	GSA	PS	PSO	TSO
1	I_{ph}	5.300 A	7.45 A	7.21 A	6.95 A	6.45 A	6.06 A	5.41 A
2	I_{01}	8.97×10^{-9} A	9.48×10^{-9} A	9.27×10^{-9} A	9.27×10^{-9} A	9.027×10^{-9} A	9.17×10^{-9} A	8.7×10^{-9} A
3	I_{02}	9.29×10^{-7} A	10.88×10^{-7} A	10.49×10^{-7} A	9.87×10^{-7} A	10.22×10^{-7} A	10.98×10^{-7} A	9.29×10^{-7} A
4	R_s	0.896 Ω	1.12 Ω	1.176 Ω	1.0968 Ω	1.796 Ω	1.016 Ω	0.942 Ω
5	R_p	1298.18 Ω	1498.58 Ω	1545.08 Ω	1434.78 Ω	1398.18 Ω	1386.08 Ω	1281.98 Ω
6	a_1	1	1.88	1.76	1.63	1.43	1.19	1.01
7	Time (s)	…	898	731	676	487	341	228

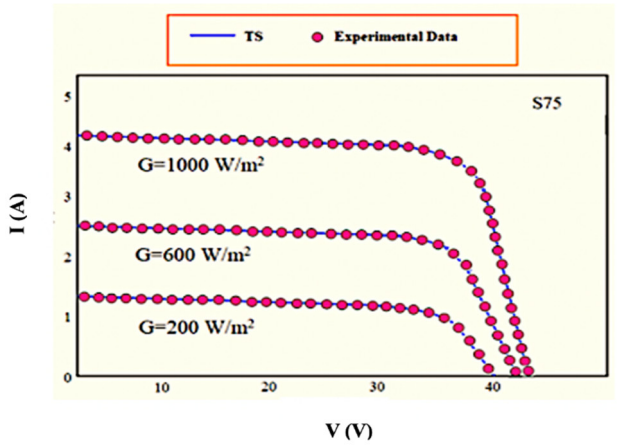

(**a**)

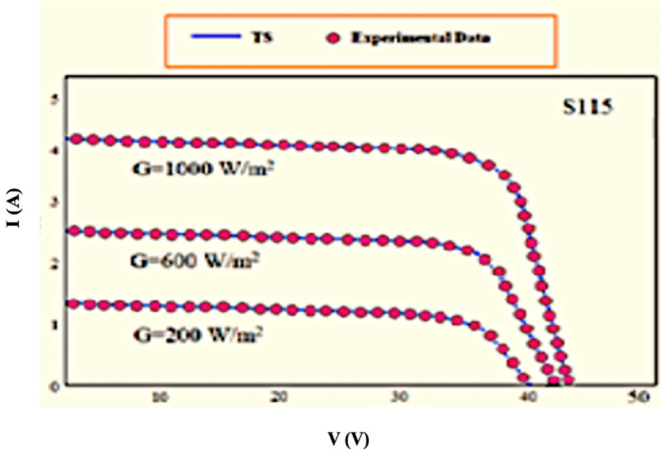

(**b**)

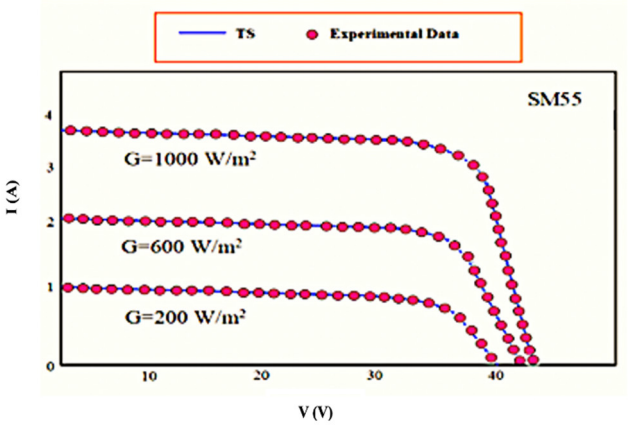

(**c**)

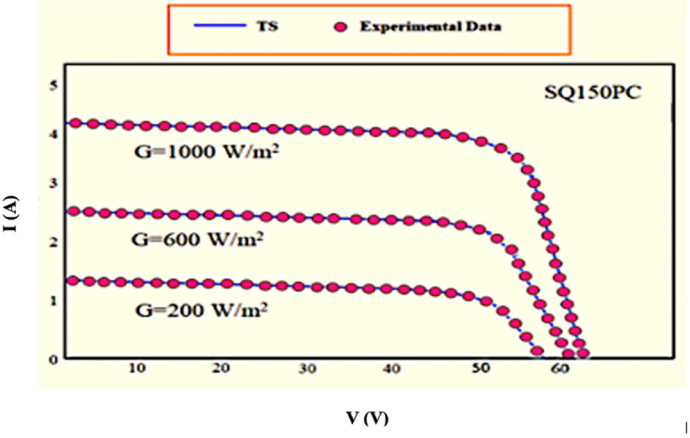

(**d**)

Figure 5. I–V qualities obtained by utilizing TSO calculation and trial information. (**a**) S75, (**b**) S115, (**c**) SM55, and (**d**) SQ150PC.

At various irradiance levels, including 1000 W/m² and 600 W/m², the TSO approach was utilized to inspect the effects of a few PV modules, including multi-glasslike (S75 and S115) and mono-translucent (SM55 and SQ150PC). The S75 multi-crystalline panel takes 0.5 s to compute at 1000 W/m² to retrieve the parameters. Different modules, such as S115, SM55, and SQ 150PC, require 0.43, 0.41, and 0.39 s, respectively. Data extracted is tabulated in Table 3. The extra boundaries of the S75 PV module, I_{Ph}, I_{01}, I_{02}, R_S, R_P, and a1, are 5.420 A, 9.97×10^{-9} A, 6.29×10^{-7} A, 0.696 Ω, 416.18 Ω, and 1.15. At G = 600 W/m². The situation is therefore similar. The S75 modules take up a significant amount of processing time, whereas the SM55 takes up the least. However, the S75 multi-crystalline module's total numerical values are noticeable under any irradiance levels.

Table 3. Data extracted at different irradiance levels from multi-crystalline and mono-crystalline.

S. NO	Parameter	Multi-Crystalline		Mono-Crystalline	
G = 1000 W/m²		***S75***	***S115***	***SM55***	***SQ150PC***
1	I_{Ph}(A)	5.420	5.457	3.876	4.046
2	I_{01} (A)	9.97×10^{-9}	10.87×10^{-9}	1.68×10^{-9}	2.47×10^{-9}
3	I_{02} (A)	6.29×10^{-7}	6.37×10^{-7}	2.98×10^{-7}	3.049×10^{-7}
4	Rs (Ω)	0.696	0.968	0.32	0.876
5	Rp (kΩ)	416.18	434.78	598.58	345.08
6	a_1	1.15	1.23	1.08	1.76
7	Time (min)	0.5	0.43	0.41	0.39
G = 600 W/m²					
1	I_{Ph}(A)	3.420	3.457	3.876	2.546
2	I_{01} (A)	10.09×10^{-9}	8.87×10^{-9}	3.68×10^{-9}	8.47×10^{-9}
3	I_{02} (A)	8.29×10^{-7}	6.37×10^{-7}	2.98×10^{-7}	3.029×10^{-7}
4	Rs (Ω)	0.596	0.698	0.52	0.976
5	Rp (kΩ)	426.18	464.38	698.58	1345.08
6	a_1	1.15	1.13	1.28	1.36
7	Time (min)	0.41	0.36	0.36	0.39

The combination time for the TSO technique corresponds to the level of emphasis performed. As the quantity of cycles rises, so do the execution time and the rate at which the results increase. Instances of the combination reaction of PV modules with 40-watt and 200-watt appraisals are displayed in Figure 6a,b.

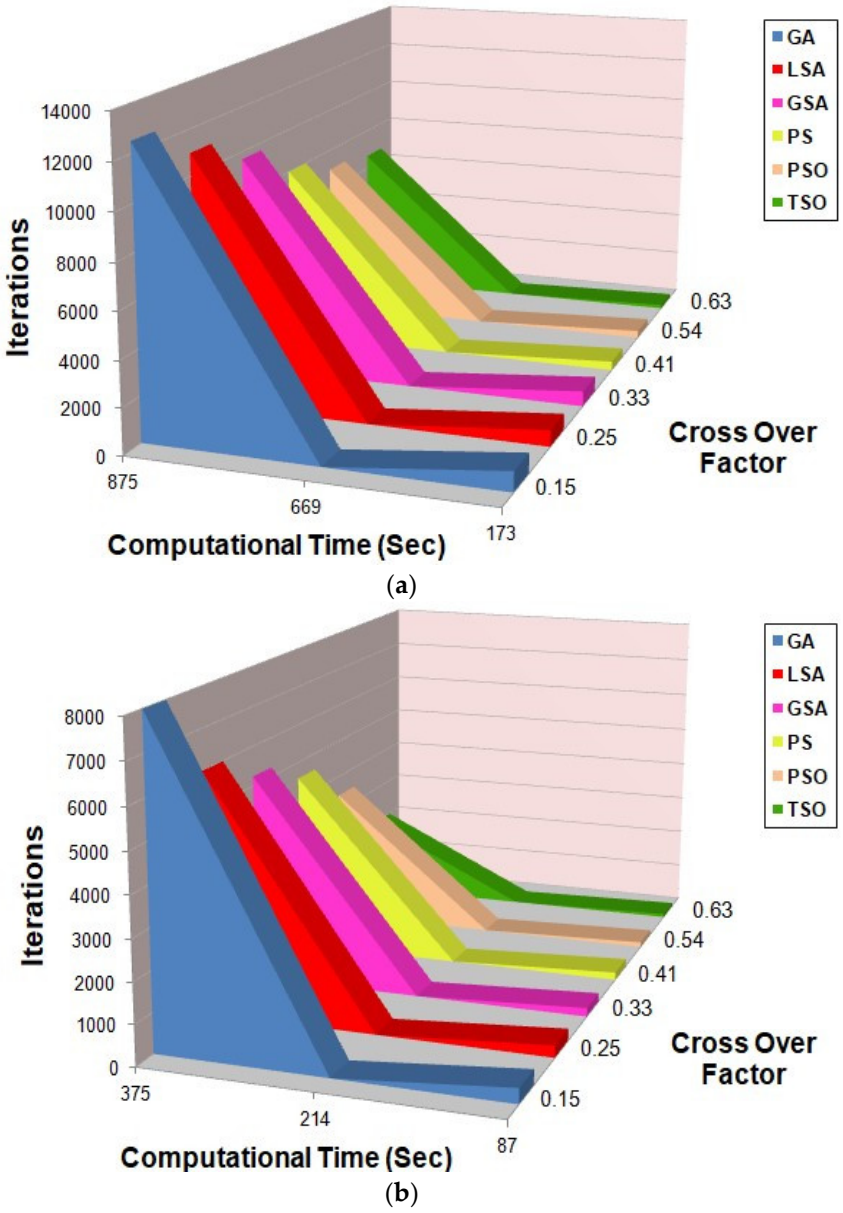

Figure 6. Convergence characteristics of (**a**) 40-watt and (**b**) 200-watt PV module.

Changes in absolute errors have a significant impact on the proposed TSO algorithm and current approaches under diverse irradiance patterns. Figure 7a,b illustrates the % absolute error on the mono-crystalline and multi-crystalline PV panels, respectively.

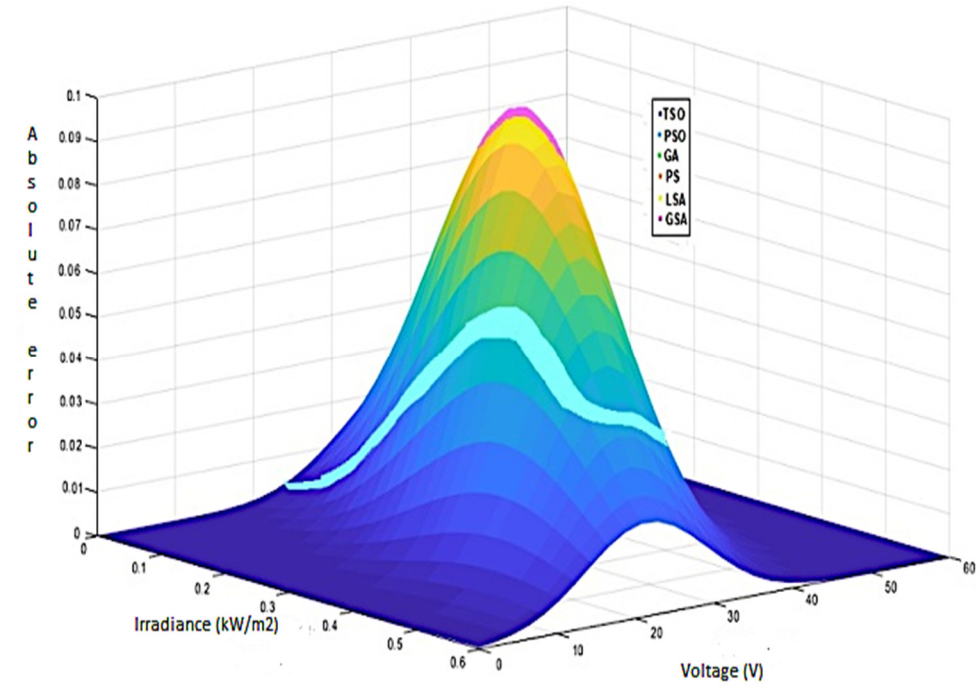

(**a**)

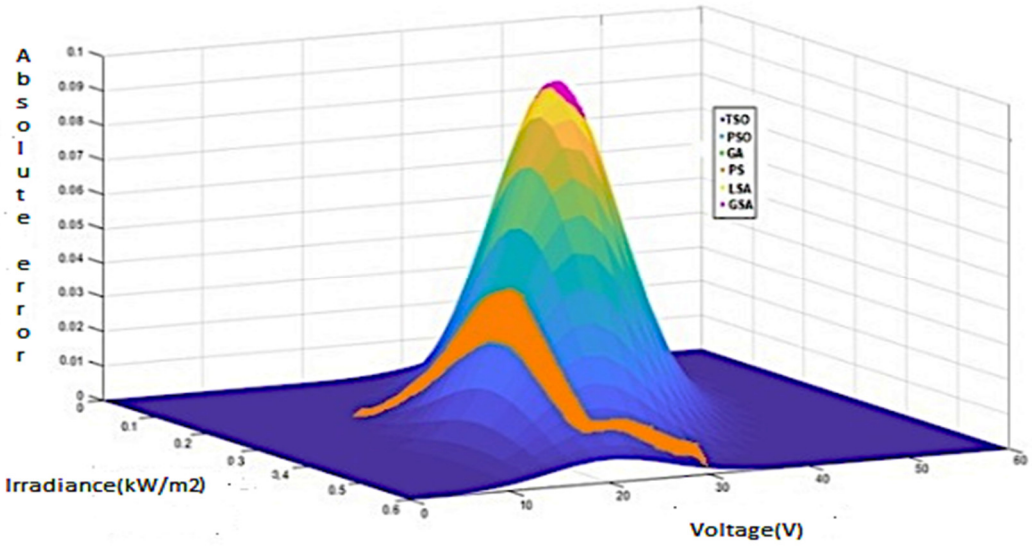

(**b**)

Figure 7. Absolute errors for (**a**) multi-crystalline and (**b**) mono-crystalline.

6. Conclusions

Under a variety of environmental conditions, the parasitic limits of PV modules may be extricated using a TSO-based approach. On an assortment of PV modules, including 40-watt and 200-watt PV modules, multi-glass-like mono clear, and small-film modules, the proposed TSO algorithm was compared with existing computation algorithms, such as the genetic algorithm, lightning search algorithm, gravitational search algorithm, pattern search algorithm (PS), and particle swarm optimization (PSO). The proposed approach is different from the other current optimization algorithms, and showed a superior calculation ability proving that the TSO calculation has superior qualities, with less intricacy and quicker combination, as displayed in Tables 1 and 2.

Author Contributions: Conceptualization, N.B.R., P.S. and S.R.K.; Data curation, N.B.R. and P.S.; Formal analysis, S.R.K. and N.R.; Funding acquisition, L.M.-P.; Investigation, N.R.; Software, N.B.R.; Supervision, N.R.; Writing—original draft, N.B.R. and P.S.; Writing—review & editing, L.M.-P. All authors have read and agreed to the published version of the manuscript.

Funding: This research received no external funding.

Conflicts of Interest: The authors declare no conflict of interest.

Nomenclature

I_{PV}	photovoltaic current (A)
I_S	diode reverse-saturation current (A)
I_d	diode currents (A)
I_{ph}	photocurrent (A)
q	charge (C)
α	number of iterations for each simplex
β	number of offspring
R_s	series resistance (Ω)
R_{sh}	shunt resistance (Ω)
K_b	Boltzmann constant ($1.3806503 \times 10^{-23}$ J/K
η	empirical constant 1 for Ge,2 for Si
T_K	cell temperature in kelvin

References

1. Bhukya, M.N.; Kumar, M.; Mohan, V.C.J. Design and Development of a Low-Cost Grid Connected Solar Inverter for Maximum Solar Power Utilization. In *Recent Advances in Power Electronics and Drives*; Lecture Notes in Electrical Engineering; Springer: Singapore, 2021; Volume 707. https://doi.org/10.1007/978-981-15-8586-9_37.
2. Bae, Y.; Vu, T.; Kim, R. Implemental Control Strategy for Grid Stabilization of Grid-Connected PV System Based on German Grid Code in Symmetrical Low-to-Medium Voltage Network. *IEEE Trans. Energy Convers.* **2013**, *28*, 619–631. https://doi.org/10.1109/TEC.2013.2263885.
3. Ali, A.; Almutairi, K.; Padmanaban, S.; Tirth, V.; Algarni, S.; Irshad, K.; Islam, S.; Zahir, M.H.; Shafiullah, M.; Malik, M.Z. Investigation of MPPT Techniques Under Uniform and Non-Uniform Solar Irradiation Condition–A Retrospection. *IEEE Access* **2020**, *8*, 127368–127392. https://doi.org/10.1109/ACCESS.2020.3007710.
4. Ahmad, W.; Liu, D.; Wu, J.; Ahmad, W.; Wang, Y.; Zhang, P.; Zhang, T.; Zheng, H.; Chen, L.; Chen, Z.D.; et al. Enhanced Electrons Extraction of Lithium-Doped SnO2Nanoparticles for Efficient Planar Perovskite Solar Cells. *IEEE J. Photovolt.* **2019**, *9*, 1273–1279. https://doi.org/10.1109/JPHOTOV.2019.2924734.
5. Villalva, M.G.; Gazoli, J.R.; Filho, E.R. Comprehensive Approach to Modeling and Simulation of Photovoltaic Arrays. *IEEE Trans. Power Electron.* **2009**, *24*, 1198–1208. https://doi.org/10.1109/TPEL.2009. 2013862.
6. Arefifar, S.A.; Paz, F.; Ordonez, M. Improving Solar Power PV Plants Using Multivariate Design Optimization. *IEEE J. Emerg. Sel. Top. Power Electron.* **2017**, *5*, 638-650. https://doi.org/10.1109/JESTPE.2017.2670500.
7. Kumar, N.; Saha, T.K.; Dey, J. Sliding-Mode Control of PWM Dual Inverter-Based Grid-Connected PV System: Modeling and Performance Analysis. *IEEE J. Emerg. Sel. Top. Power Electron.* **2015**, *4*, 435–444. https://doi.org/10.1109/JESTPE.2015.2497900.
8. Ma, X.; Huang, W.-H.; Schnabel, E.; Kohl, M.; Brynjarsdottir, J.; Braid, J.L.; French, R.H. Data-Driven II–VV Feature Extraction for Photovoltaic Modules. *IEEE J. Photovolt.* **2019**, *9*, 1405–1412. https://doi.org/10.1109/JPHOTOV.2019.2928477.
9. Saleem, H.; Karmalkar, S. An Analytical Method to Extract the Physical Parameters of a Solar Cell from Four Points on the Illuminated J-V Curve. *IEEE Electron Device Lett.* **2009**, *30*, 349–352. https://doi.org/10.1109/LED.2009.2013882.
10. Soeriyadi, A.H.; Wang, L.; Conrad, B.; Li, D.; Lochtefeld, A.; Gerger, A.; Barnett, A.; Perez-Wurfl, I. Extraction of Essential Solar Cell Parameters of Subcells in a Tandem Structure With a Novel Three-Terminal Measurement Technique. *IEEE J. Photovolt.* **2017**, *8*, 327–332. https://doi.org/10.1109/JPHOTOV.2017.2762596.
11. Mintairov, M.; Kalyuzhnyy, N.A.; Evstropov, V.V.; Lantratov, V.M.; Mintairov, S.A.; Shvarts, M.Z.; Andreev, V.M.; Luque, A. The Segmental Approximation in Multijunction Solar Cells. *IEEE J. Photovolt.* **2015**, *5*, 1229–1236. https://doi.org/10.1109/JPHOTOV.2015.2416006.
12. Wei, T.; Yu, F.; Huang, G.; Xu, C. A Particle-Swarm-Optimization-Based Parameter Extraction Routine for Three-Diode Lumped Parameter Model of Organic Solar Cells. *IEEE Electron Device Lett.* **2019**, *40*, 1511–1514. https://doi.org/10.1109/LED.2019.2926315.
13. Bhukya, M.N.; Kumar, M.; Depuru, S.R. A Simple Approach to Enhance the Performance of Traditional P&O Scheme under Partial Shaded Condition by Employing Second Stage to the Existing Algorithm. In *Modeling, Simulation and Optimization*; Springer: Singapore, 2021. https://doi.org/10.1007/978-981-15-9829-6_43.

14. Diab, A.A.Z.; Sultan, H.M.; Aljendy, R.; Al-Sumaiti, A.S.; Shoyama, M.; Ali, Z.M. Tree Growth Based Optimization Algorithm for Parameter Extraction of Different Models of Photovoltaic Cells and Modules. *IEEE Access* **2020**, *8*, 119668–119687. https://doi.org/10.1109/ACCESS.2020.3005236.
15. Bhukya, M.N.; Kota, V.R.; Depuru, S.R. A Simple, Efficient, and Novel Standalone Photovoltaic Inverter Configuration With Reduced Harmonic Distortion. *IEEE Access* **2019**, *7*, 43831–43845. https://doi.org/10.1109/ACCESS.2019.2902979.
16. Raba, A.; Leroy, Y.; Kohlstädt, M.; Würfel, U.; Cordan, A. Organic Solar Cells: Extraction of Physical Parameters by Means of Markov Chain Monte Carlo Techniques. *IEEE J. Photovolt.* **2017**, *7*, 1098–1104. https://doi.org/10.1109/JPHOTOV.2017.2690876.
17. Caracciolo, F.; Dallago, E.; Finarelli, D.G.; Liberale, A.; Merhej, P. Single-Variable Optimization Method for Evaluating Solar Cell and Solar Module Parameters. *IEEE J. Photovolt.* **2012**, *2*, 173–180. https://doi.org/10.1109/JPHOTOV.2011.2182181.
18. Cervellini, M.P.; Echeverria, N.I.; Antoszczuk, P.D.; Retegui, R.A.G.; Funes, M.A.; Gonzalez, S.A. Optimized Parameter Extraction Method for Photovoltaic Devices Model. *IEEE Lat. Am. Trans.* **2016**, *14*, 1959–1965. https://doi.org/10.1109/TLA.2016.7483540.
19. Semero, Y.K.; Zhang, J.; Zheng, D. PV power forecasting using an integrated GA-PSO-ANFIS approach and Gaussian process regression based feature selection strategy. *CSEE J. Power Energy Syst.* **2018**, *4*, 210–218. https://doi.org/10.17775/CSEEJPES.2016.01920.
20. Bhukya, M.N.; Kumar, M. Factors Affecting the Efficiency of Solar Cell and Technical Possible Solutions to Improve the Performance. In *Modeling, Simulation and Optimization*; Springer, Singapore, 2021; pp. 623–634. https://doi.org/10.1007/978-981-15-9829-6_49.
21. Liao, Z.; Gu, Q.; Li, S.; Hu, Z.; Ning, B. An Improved Differential Evolution to Extract Photovoltaic Cell Parameters. *IEEE Access* **2020**, *8*, 177838–177850. https://doi.org/10.1109/ACCESS.2020.3024975.
22. Toledo, F.J.; Blanes, J.M.; Galiano, V. Two-Step Linear Least-Squares Method for Photovoltaic Single-Diode Model Parameters Extraction. *IEEE Trans. Ind. Electron.* **2018**, *65*, 6301–6308. https://doi.org/10.1109/TIE.2018.2793216.
23. Rossmo, K.; Harries, K. A novel P&OT-Neville's interpolation MPPT scheme for maximum PV sytem energy extraction. *Int. J. Renew. Energy Dev.* **2021**, *7*, 251–260. https://doi.org/10.1 4710/ijred.7.3.
24. AlShabi, M.; Ghenai, C.; Bettayeb, M.; Ahmad, F.F.; Assad, M.E.H. Multi-group grey wolf optimizer (MG-GWO) for estimating photovoltaic solar cell model. *J. Therm. Anal.* **2020**, *144*, 1655–1670. https://doi.org/10.1007/s10973-020-09895-2.
25. Manda, P.K.; Ramaswamy, S.; Dutta, S. Extraction of the Built-in Potential for Organic Solar Cells from Current–Voltage Characteristics. *IEEE Trans. Electron Devices* **2017**, *65*, 184–190. https://doi.org/10.1109/TED.2017.2773708.
26. Kota, V.R.; Bhukya, M.N. A simple and efficient MPPT scheme for PV module using 2-Dimensional Lookup Table. In Proceedings of the 2016 IEEE Power and Energy Conference at Illinois (PECI), Urbana, IL, USA, 19–20 February 2016; pp. 1–7. https://doi.org/10.1109/PECI.2016.7459226.
27. Bauer, A.; Hanisch, J.; Ahlswede, E. An Effective Single Solar Cell Equivalent Circuit Model for Two or More Solar Cells Connected in Series. *IEEE J. Photovolt.* **2013**, *4*, 340–347. https://doi.org/10.1109/JPHOTOV.2013.2283056.
28. Azizi, A.; Logerais, P.-O.; Omeiri, A.; Amiar, A.; Charki, A.; Riou, O.; Delaleux, F.; Durastanti, J.-F. Effect of the maturing of a photovoltaic module on the presentation of a framework associated framework. *Sol. Energy* **2018**, *174*, 445–454; ISSN 0038-092X. https://doi.org/10.1016/j.solener.2018.09.022.